Design Considerations for a Semi-Active Electromagnetic Suspension System

Johannes J. H. Paulides, Laurentiu Encica, Elena A. Lomonova, and Andre J. A. Vandenput

Electromechanics and Power Electronics Group, Eindhoven University of Technology, 5600 MB Eindhoven, The Netherlands

Vehicle manufacturers always strive to improve the vehicle handling and passenger safety and comfort. One of the focus points for the automotive industry is the (semi-)active suspension system for which various commercial technologies are existing, varying from pneumatic to hydraulic. This paper addresses the design considerations of a tubular electromagnetic actuator for semi-active suspension.

***Index Terms*—Design optimization, permanent magnet actuators, road vehicle power systems, space mapping.**

I. Introduction

TYPICAL vehicle behavior is diving to the front during braking (pitching) and leaning over during cornering (rolling). Additionally, vertical vibrations (bouncing) of the vehicle body can occur while driving over road irregularities. This has an adverse effect on passenger comfort and can even cause a potential safety risk, since the tires might lose road grip. The vehicle suspension has to ensure ride comfort and road holding for a variety of road conditions and vehicle maneuvers. Only a compromise between these two conflicting criteria can be obtained with a passive solution such as fixed rates springs and dampers. However, a semi-active suspension system [1], as shown in Fig. 1, characterized by a built-in actuator, can generate control forces to suppress the roll and pitch motions and can ameliorate both safety and comfort. In addition road holding can be improved, due to advanced tire technology and road contact forces control, since it can eliminate the low frequency resonance of the vehicle body (typically 1–2 Hz).

In order to obtain good performance, it is necessary for the actuator control bandwidth to extend substantially beyond the wheel-hop natural frequency (typically 10–15 Hz). These active systems need such a high bandwidth because the vibrations of the unsprung mass (initiated by the road irregularities) have to be absorbed actively unlike the slow passive systems. This paper describes an electromagnetic actuator design for semi-active suspension system (Fig. 1) in order to minimize the articulation during a slalom maneuver.

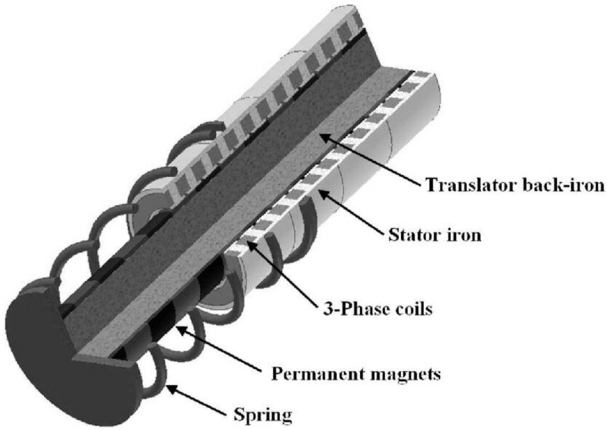

Fig. 1. Schematic of a semi-active suspension system.

II. Quarter Car Model

A well established means of evaluating the performance of a suspension system is the use of a quarter car model, as shown in Fig. 2, since it provides a proper representation of controlling wheel load variations and suspension working space. In this model all the various components are assumed to be linear, even though in practice the various passive components are neither linear nor symmetrical.

The quarter-car model contains two vertical degrees of freedom: 1) the unsprung mass, M_w and 2) the sprung mass,

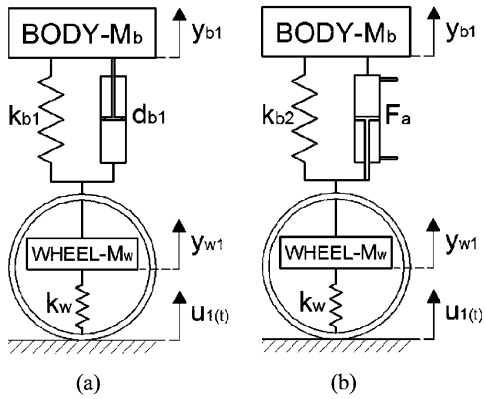

Fig. 2. Schematic of (a) passive and (b) semi-active suspension system as quarter-car model representation.

M_b, displacements. The body and wheel movements are specified by y_{b1} and y_{w1}, the passive spring stiffness by k_{b1} and k_{b2}, the passive damper coefficient by d_{b1}, the actuator force by F_a, and the road displacement by $u_1(\mathrm{t})$. The various system parameters for the suspension are summarized in Table I.

III. Actuator Position

In order to minimize the energy consumption, space envelope, and costs, several semi-active suspension configurations

Digital Object Identifier 10.1109/TMAG.2006.879963

TABLE I
MECHANICAL SUSPENSION PROPERTIES

Quarter body mass	M_b	400 kg
Wheel mass	M_w	40 kg
Spring stiffness	k_{bl}	25 kN/m
Damper coefficient	d_{bl}	1.2 kN/m/s
Tire stiffness	k_{wl}	160 kN/m

exist, where in general this means a combination of an actuator with passive elements. For example, to minimize the energy consumption, the actuator can be placed in series/parallel [k_{sp1} and k_{sp2}; Fig. 3(a)] or parallel [k_{pa}; Fig. 3(b)] with a conventional mechanical spring. In both configurations, a reduced actuator force is needed since the vehicle static weight is carried by the spring. The series/parallel configuration [Fig. 3(a)] requires a relatively low-bandwidth actuator force, which is most commonly used in combination with hydraulics. The parallel configuration [Fig. 3(b)] is a high-bandwidth suspension, since the actuator must be able to reach the bandwidth of the total system to control the road motions effectively. For both semi-active suspensions the average power consumption can be improved by including a damper, albeit that a higher power level is needed for high acceleration movements.

Cech [2] showed that, in comparison to passive systems, using the series/parallel configuration even a limited actuator bandwidth of 1 Hz already resulted in a considerable improvement in ride comfort. However, for further improvement the parallel configuration [Fig. 3(b)] is chosen, since it fully benefits from the high bandwidth of the direct-drive electromagnetic actuator and excludes the extra force, complexity, and delay introduced by k_{sp2}.

IV. SLALOM MANEUVER

The specific focus of this paper is to be able to minimize the articulation for a slalom maneuver with the cones 45 m apart, driving at a speed of 30 km/h. The force amplitude is taken from a semi-circle between the cones, therefore

$$F_{\mathrm{susp}} = \frac{\sum_{n=1}^{4} M_{b,n} v^2}{R_{\mathrm{sl}}} \tag{1}$$

where v is the vehicle speed in m/s, and R_{sl} is the radius of the semi-circle in m. Using the quarter-car model and the numbers of Table I, a force level of ≈4900 N is needed for the total vehicle. This being equivalent to a force level of ≈1225 N per actuator, disregarding any anti-roll bar in the system. Further, this assumes that the roll center and center of gravity are the same, actuator placement in line with the wheel and half the track width equal to the height of the center of gravity, hence, a worst case condition for this maneuver.

V. TUBULAR ACTUATOR DESIGN

A three-phase direct-drive slotted tubular brushless linear permanent magnet (PM) machine [Figs. 1 and 3(b)] is chosen. This topology incorporates a high force density, which makes it an attractive candidate for applications where volume and reliability are crucial.

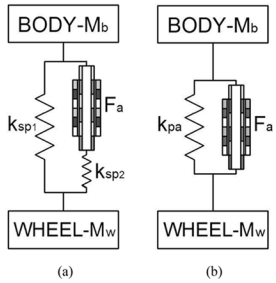

Fig. 3. (a) Series/parallel and (b) parallel semi-active suspension configurations.

TABLE II
ACTUATOR SIZES FOR VARIOUS POLE-PAIRS

Force level (N)	205 (I)	245 (I)	310 (I)	410 (I)	615 (I)	**245 (II)**
Pole-pairs	6	5	4	3	2	**5**
h_1 (mm)	5.0	5.0	5.0	5.8	5.0	**10.3**
h_2 (mm)	22.0	23.3	25.1	27.5	31.4	**16.7**
h_3 (mm)	5.0	5.0	5.0	5.0	5.0	**5.0**
h_4 (mm)	1	1	1	1	1	**1**
h_5 (mm) $= 2h_4$	2.0	2.0	2.0	2.0	2.0	**2.0**
h_6 (mm)	20.7	22.5	25.2	27.8	34.2	**31.3**
h_7 (mm)	7.4	7.8	8.4	9.2	10.5	**5.8**
r_t (mm) (total radius)	63.1	66.6	71.7	78.3	89.1	**72.0**
l_1 (mm)	2.8	3.0	3.2	3.6	4.0	**2.2**
l_2 (mm)	14.7	15.5	16.7	18.3	20.9	**11.2**
l_3 (mm) $= l_2 + 1.2l_1$	18.1	19.1	20.6	22.6	25.8	**13.7**
l_4 (mm)	61.1	64.6	69.7	76.2	87.0	**46.4**
l_t (mm) (total length)	366.6	322.5	278.8	228.6	174.0	**232.0**
F_{dens} (kN/m^3)	210	214	218	220	224	**255**
T_{peak} (°C)	116	123	134	144	167	**156**

The analytical determination of the machine performance is commonly used for the design optimization and dynamic modeling of linear permanent magnet machines. However, model inaccuracies form a problem, especially when flux leakage, fringing effects, or magnetic saturation are significant. The magnetic field distribution can be established accurately by finite element (FE) analysis, but the process is time demanding and is rather inefficient for design optimization. Therefore, a space mapping (SM) optimization technique [3] is considered for deriving the actuator design, since it combines the advantages of the two analysis methods mentioned above. SM speeds up the design procedure by exploiting a combination of fast, less accurate (*coarse*) models and time expensive, accurate (*fine*) models. The misalignment between the coarse and fine models is corrected by means of a mapping function, which is iteratively updated. The algorithm used in this paper is detailed in [4].

The actuator geometry is obtained by size optimization, having as objective the force density maximization for the required force output of the 1225 N. Five configurations with different number of pole-pairs are introduced and, in order to reduce the time needed for model evaluation, only one pole-pair is considered, with the corresponding force levels summarized in Table II. The geometry of one pole-pair is defined in Fig. 4. The number of independent (optimization) variables is fixed to four: the length of the magnets (h_3), the radius that defines the

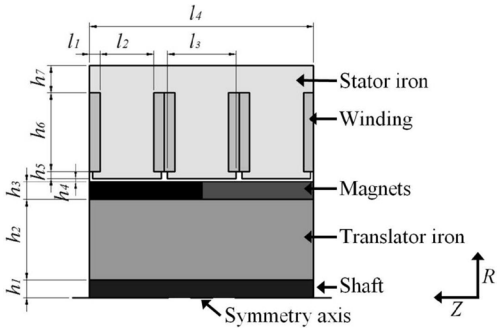

Fig. 4. Geometry of the tubular actuator (one pole-pair).

middle of the air-gap ($r_g = h_1 + h_2 + h_3 + h_4/2$), the axial length ($l_4$) and the peak Ampère turns (NI_p). The remaining parameters are derived based on the following model assumptions: the current density is fixed to 15 A/mm^2, the coil packing factor is taken 0.5, the air-gap length h_4 is 1 mm, the NdFeB PM has a remanent flux density of 1.23 T, and the flux densities in the stator and translator back iron are 1.4 T.

The total static actuator force, for the coarse analytical model, is calculated as the sum of the generated forces for each phase [5]

$$F_a = -\frac{\sqrt{2}\pi}{\tau_p} N I_p \left[\sin\left(\frac{\pi}{\tau_p}x\right) \sum_{n=1}^{\infty} n\, K_{wn} \times \Phi_n \sin\left(\frac{\pi}{\tau_p} n x\right) + \sin\left(\frac{\pi}{\tau_p}\left(x + \frac{2}{3}\tau_p\right)\right) \sum_{n=1}^{\infty} n\, K_{wn} \times \Phi_n \sin\left(\frac{\pi}{\tau_p} n \left(x + \frac{2}{3}\tau_p\right)\right) + \sin\left(\frac{\pi}{\tau_p}\left(x - \frac{2}{3}\tau_p\right)\right) \times \sum_{n=1}^{\infty} n\, K_{wn} \Phi_n \sin\left(\frac{\pi}{\tau_p} n \left(x - \frac{2}{3}\tau_p\right)\right)\right] \quad (2)$$

where F_a is the actuator force, τ_p is the magnet pole pitch, NI_p is the amount of Ampère turns per coil, K_{wn} is the winding factor of the nth dimension high harmonic wave component, Φ_n is the nth dimension component of inter-linkage magnetic flux, and x is the translator displacement.

The fine model is an axial-symmetric, magnetostatic, FE model. It needs mentioning that the 12 V level in automotive applications is still ambiguous for the introduction of electromagnetic suspension. The dynamic modeling needed to investigate this has not been considered in this paper. The actuator is therefore modeled in a locked position, hence a magnetostatic FE model.

The lower, L_b, and upper, U_b, constraints for the optimization variables are given by L_b =[5 mm, 10 mm, 10 mm, 1 A] and U_b = [50 mm, 200 mm, 400 mm, 30 A], where the total radius is constrained to be no larger than the axial length of the pole-pair. It needs noting that the solutions should be considered only as local optima.

Table II summarizes the results obtained for the five chosen configurations. The force density is calculated as the ratio between the force output level and the rectangular domain circumscribed to the tubular actuator. A thermal FE analysis is performed for each design to determine the value of the hot-spot temperature in the actuator, using adiabatic conditions on the model's left- and right-hand sides, a convection boundary on the outer surface of 50 Wm^{-2}K^{-1}, and an ambient temperature of 25 °C.

It needs to be noted that, further to the assumed adiabatic conditions, the temperature is calculated for continuous operation, while the actuator in practice has a reduced duty cycle and hence the operating temperature would be at a decreased level. The space envelope of a mechanical suspension spring is defined by a diameter of approximately 140–150 mm. Table II shows that the 5 and 6 pole-pair designs could be resized since their diameters are smaller than the available space. As an example, the redesigned 5 pole-pair actuator (given in the last column of Table II) provides a force density of 255 kN/m^3, however, at the expense of an increased hot-spot temperature.

VI. Conclusion

A comparative study of different actuator configurations shows that the brushless PM tubular actuator is a viable choice for a semi-active suspension system. The design 310(I) in Table II exhibits 218 kN/m^3 for a ΔT of 100 °C, which approaches the level mentioned by Wang *et al.* [6]. It needs to be mentioned that the obtained designs can be improved, since only a restricted number of design variables was considered. In the semi-active suspension application a reduced duty-cycle is applicable, hence, and increased force density of 255 kN/m^3 can be achieved as summarized by 245(II) in Table II.

Acknowledgment

This work was sponsored by SenterNovem (agency of the Dutch ministry of economical affairs), SKF Automotive and TNO Research Automotive, the Netherlands.

References

[1] W. D. Jones, "Easy ride: Bose Corp. uses speaker technology to give cars adaptive suspension," *IEEE Spectr.*, vol. 42, no. 5, pp. 12–14, May 2005.

[2] I. Cech, "A slow acting in series active suspension," *Veh. Syst. Dyn.*, vol. 16, pp. 17–26, 1987.

[3] J. W. Bandler, Q. S. Cheng, S. A. Dakroury, A. S. Mohamed, M. H. Bakr, K. Madsen, and J. Sondergaard, "Space mapping: The state of the art," *IEEE Trans. Microw. Theory Tech.*, vol. 52, no. 1, pp. 337–361, Jan. 2004.

[4] L. Encica, D. Echeverría, E. A. Lomonova, A. J. A. Vandenput, P. W. Hemker, and L. Lahaye, "Efficient optimal design of electromagnetic actuators using space-mapping," in *Proc. 6th World Congr. Structural and Multidisciplinary Optimization*, Rio de Janeiro, 2005, pp. 1–10.

[5] T. Mizuno and H. Yamada, "Magnetic circuit analysis of a linear synchronous motor with permanent magnets," *IEEE Trans. Magn.*, vol. 28, no. 5, pp. 3027–3029, Sep. 1992.

[6] J. Wang, G. W. Jewell, and D. Howe, "Design optimization and comparison of tubular permanent magnet machine topologies," *IEE Proc.-Electr. Power Appl.*, vol. 148, no. 5, pp. 456–464, Sep. 2001.

Manuscript received March 13, 2006 (e-mail: j.j.h.paulides@tue.nl).